ARTICLE

Mode-Specific Quantum Dynamics Study of OH+H_2S→H_2O+SH Reaction†

Haipan Xiang[a,b], Yunpeng Lu[c*], Hongwei Song[a*], Minghui Yang[a,d]

a. State Key Laboratory of Magnetic Resonance and Atomic and Molecular Physics, Innovation Academy for Precision Measurement Science and Technology, Chinese Academy of Sciences, Wuhan 430071, China
b. College of Physical Science and Technology, Huazhong Normal University, Wuhan 430079, China
c. Division of Chemistry and Biological Chemistry, School of Physical and Mathematical Sciences, Nanyang Technological University, Singapore 637371, Singapore
d. Wuhan National Laboratory for Optoelectronics, Huazhong University of Science and Technology, Wuhan 430071, China

(Dated: Received on December 14, 2021; Accepted on January 5, 2022)

The hydrogen abstraction reaction from H_2S by OH is of key importance in understanding of the causes of acid rain, air pollution, and climate change. In this work, the reaction OH+H_2S→H_2O+SH is investigated on a recently developed *ab initio*-based globally accurate potential energy surface by the time-dependent wave packet approach under a reduced-dimensional model. This reaction behaves like a barrier-less reaction at low collision energies and like an activated reaction with a well-defined barrier at high collision energies. Exciting either the symmetric or antisymmetric stretching mode of the molecule H_2S enhances the reactivity more than exciting the bending mode, which is rationalized by the coupling strength of each normal mode with the reaction coordinate. In addition, the mode-specific rate constant shows a remarkable non-Arrhenius temperature dependence.

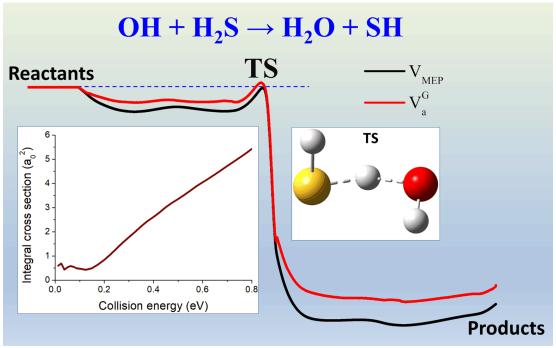

Key words: OH+H_2S reaction, Mode specificity, Quantum dynamics, Non-Arrhenius behavior

I. INTRODUCTION

The hydrogen atom abstraction reactions from polyatomic molecules that are prevalent in chemically active environments have attracted considerable attention in recent years [1−6]. Although quasi-classical trajectory (QCT) method [7] has been widely used to investigate this kind of reaction, it loses its ability in describing the dynamical behavior around the energy threshold. Because the quantum effect, such as tunneling, is expected to be important in the region. Therefore, a comprehensive description of dynamical behavior in chemical reactions can be achieved only through quantum scattering calculations.

The hydroxyl radical (OH) is an important oxidant in the upper and middle atmosphere [8]. The hydrogen abstraction reaction from H_2S by OH, a critical step in the oxidation and ignition of the molecule H_2S, plays a significant role in combustion chemistry and environmental chemistry [9−16]. The rate constants of the reaction OH+H_2S→H_2O+SH have been measured by different groups [17−23], in which an unusual temperature dependence was observed. The existence of the non-Arrhenius behavior was confirmed by several

†Part of Special Issue "In Memory of Prof. Nanquan Lou on the occasion of his 100th anniversary".
*Authors to whom correspondence should be addressed. E-mail: yplu@ntu.edu.sg, hwsong@wipm.ac.cn

levels of theoretical calculations [24−27] and attributed by Ellingson and Truhlar [26] to a submerged dynamical bottleneck through direct dynamics calculations. Butkovskaya and Setser [28, 29] measured the vibrational distributions of the products H_2O (HDO) formed by the reaction between OH (OD) and H_2S at room temperature by the infrared chemiluminescence technique.

The interaction between the reactants (products) H_2S (H_2O) and OH (SH) has attracted much attention as well [24, 27, 30−32]. High-level *ab initio* calculations predicted that both reactants and products can form complexes by either two-center three-electron hemibond or hydrogen bond [31]. The classical barrier height was computed by Tang *et al.* [32] to be 0.0048 eV using the "gold standard" CCSD(T) method at the basis set of aug-cc-pV5Z. Recently, our group developed a globally accurate full-dimensional potential energy surface (PES) for the OH+H_2S→H_2O+SH reaction, for which a total of 82680 *ab initio* points were sampled and calculated by the UCCSD(T)-F12a method with the aug-cc-pVTZ basis set [33]. The flexible fundamental invariant-neural network method [34] used in the fitting enabled us to lower the root mean square error to 4.72 meV. The vibrational state distribution of the product molecule H_2O calculated by a modified normal mode analysis method [35] were in good consistence with the experimental result, verifying the accuracy of the PES.

The minimum energy path (MEP) and vibrational adiabatic ground state energy on the PES [33] are shown in FIG. 1. There exist two minima in both the entry and exit valleys. RC-A and PC-A in the figure denote the hydrogen-bonded complexes. RC-B and PC-B represent hemi-bonded complexes. The energies of RC-A and RC-B are −0.1455 and −0.1437 eV with respect to the separated reactants. The energies of PC-A and PC-B are −0.1263 and −0.0985 eV with respect to the separated products. Interestingly, the reaction has a submerged classical barrier of −0.0050 eV relative to the reactant asymptote. When the zero-point energies (ZPEs) are included, the barrier, however, becomes positive, with a value of 0.0246 eV. The calculated integral cross section (ICS) on the PES by the QCT method was found to increase monotonically with the collision energy, implying the reaction has an activation nature [33]. The collision energy in the study was limited to the range above 3 kcal/mol (0.13 eV), far above the ZPE-corrected barrier height. When the collision energy drops down to around the threshold energy, the quantum tunneling effect would be significant. In this work, the initial state-selected time-dependent wave packet (ISSTDWP) method will be implemented to investigate the mode-specific dynamics of the reaction.

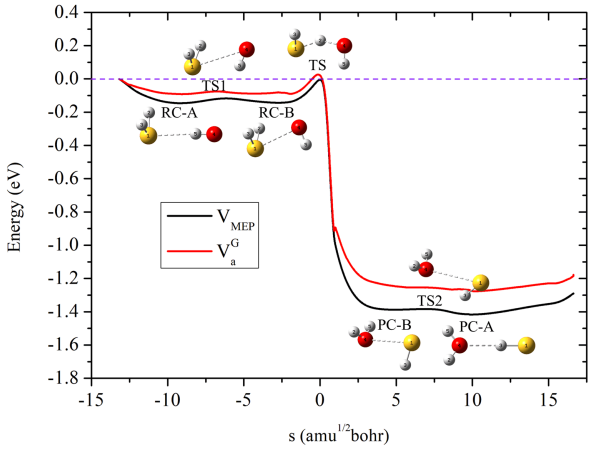

FIG. 1 Minimum energy path (V_{MEP}) and vibrational adiabatic ground state energy ($V_{\mathrm{a}}^{\mathrm{G}}$) of OH+$H_2S$→$H_2O$+SH as a function of the reaction coordinate s.

II. THEORY

The ISSTDWP approach has been detailed in Ref.[36]. We outline here the model used in this work. For the diatom-triatom reaction, the full-dimensional Hamiltonian in the Jacobi coordinates, as shown in FIG. 2, is defined as ($\hbar$=1 hereafter) [37−39]

$$\hat{H} = -\frac{1}{2\mu_R}\frac{\partial^2}{\partial R^2} - \frac{1}{2\mu_1}\frac{\partial^2}{\partial {r_1}^2} - \frac{1}{2\mu_2}\frac{\partial^2}{\partial {r_2}^2} - \frac{1}{2\mu_3}\frac{\partial^2}{\partial {r_3}^2} + \frac{\left(\hat{J}_{\mathrm{tot}} - \hat{J}\right)^2}{2\mu_R R^2} + \frac{\hat{j}_1^2}{2\mu_1 {r_1}^2} + \frac{\hat{l}_2^2}{2\mu_2 {r_2}^2} + \frac{\hat{j}_3^2}{2\mu_3 {r_3}^2} + \hat{V}\left(R, r_1, r_2, r_3, \theta_1, \theta_2, \theta_3, \varphi_1, \varphi_2\right) \quad (1)$$

where μ_R, μ_1, μ_2, and μ_3 represent the reduced masses of AB-CDE, AB, C-DE, and DE, respectively. Since the change of the bond distance of H_AO_B (r_1) along the MEP is less than 0.023 a_0 on the PES and QCT calculations proved that it behaves as a spectator bond [33], r_1 is fixed at 1.835 a_0 (the bond length of isolated OH) in the calculations. Therefore, the term $-\frac{1}{2\mu_1}\frac{\partial^2}{\partial {r_1}^2}$ in the Hamiltonian is discarded and the full-dimensional model becomes an eight-dimensional model.

DOI:10.1063/1674-0068/cjcp2112278

The parity (ε) adapted wave function of the system is expressed as

$$\psi^{J_{\rm tot}M\varepsilon}\left(\vec{R},\vec{r}_1,\vec{r}_2,\vec{r}_3\right)=\sum_{n,v,j,K}F_{nvjK}^{J_{\rm tot}M\varepsilon}u_n^{v_2}\left(R\right)\phi_{v2}\left(r_2\right)\phi_{v3}\left(r_3\right)\Phi_{jK}^{J_{\rm tot}M\varepsilon}\left(\hat{R},\hat{r}_1,\hat{r}_2,\hat{r}_3\right) \quad (2)$$

where n labels the translational basis functions along the coordinate R, v_i represents the vibrational basis index of ϕ_{vi} along the coordinate r_i (i=2,3), j denotes the composite rotational indices (j_1, l_2, j_3, j_{23}, J). Since an L-shaped grid [40] is employed in the calculations, the translational basis function, $u_n^{v_2}$, is related to v_2. The definitions of translational basis function $u_n^{v_2}$, vibrational basis function ϕ_{vi}, and rotational basis function $\Phi_{jK}^{J_{\rm tot}M\varepsilon}$ refer to Ref.[39].

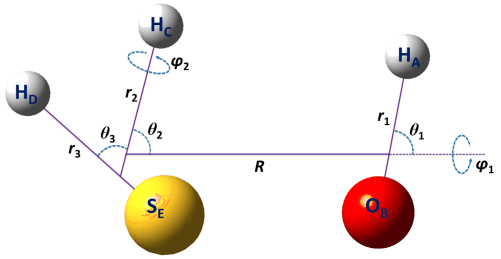

FIG. 2 The full-dimensional Jacobi coordinates used for the diatom-triatom collision system.

The centrifugal sudden approximation [41, 42], in which the coupling between different K blocks is neglected, is applied in the calculations. The initial wave packet is propagated by the second-order split-operator method [43]. Negative imaginary absorbing potentials are used at the grid edges to reflect artificial boundary reflections. The initial state-specific total reaction probability is calculated by the flux operator approach [44]. Since this work is concentrated on the effect of the reactant vibrational excitation, the reactants OH and H_2S both are initially from the ground rotational states.

III. RESULTS AND DISCUSSION

The numerical parameters that are well tested in quantum dynamics (QD) calculations are given in Table I. 130 sine discrete variable representation (DVR) basis functions/grid points along the scattering coordinate R are used in the range from 2.0 a_0 to 11.5 a_0 and 48 of them are placed in the interaction region from 2.0 a_0 to 5.5 a_0. 23 potential optimized DVR (PODVR) basis functions/grid points along the radial coordinate r_2 are employed in the interaction region from 1.45 a_0 to 5.0 a_0 and 3 in the asymptotic region. The number of PODVR basis functions/grid points along r_3 is taken to be 3. The size of rotational basis is determined by $j_{1\rm max}$=20, $j_{2\rm max}$=32, $j_{3\rm max}$=26, $j_{23\rm max}$=36 and $J_{\rm max}$=30, for a grand total of 1035587. The propagation requires around 30000 a.u. The time step is set to be 10 a.u.

FIG. 3 shows the calculated reaction probabilities of OH+H_2S(n_1, n_2, n_3)→H_2O+SH with the collision energy ranging from 0.0125 eV to 0.8 eV. When the reactants are launched from the ground ro-vibrational states, as shown in the upper-left panel of FIG. 3, the reaction probability with $J_{\rm tot}$=0 does not have an energy threshold. Instead, there exists a plateau in the probability curve from 0.0125 eV to around 0.1 eV. As the collision energy further increases, the probability starts to go up monotonically. The ZPE-corrected barrier of the reaction is 0.0246 eV. The remarkable reaction probability at the collision energy below 0.0246 eV originates definitely from the quantum tunneling effect. The plateau, however, persists up to around 0.1 eV. The shallow wells in the entrance valley are likely to play a key role in forming the plateau. QCT calculations on other similar systems have found that many of the trajectories captured by shallow wells at low collision energies ultimately return back to the reactant valley due to the stereodynamics effect, *i.e.*, the reaction requires that the reactants are in a particular orientation to produce an effective collision [45−50]. With the increasing of the total angular momentum, the centrifugal potential starts to dominate the reaction and an energy threshold gradually emerges.

The reaction probability for exciting each fundamental mode of H_2S is plotted in FIG. 3 as well. When the bending mode (010) is excited, the probability curve of

DOI:10.1063/1674-0068/cjcp2112278

TABLE I Numerical parameters used in the quantum dynamics calculations for the reaction OH+H_2S→H_2O+SH (unless otherwise stated, atomic units are used).

Item	Parameters
Grid/basis range and size	R∈[2.0, 11.5]
	$N_R^{\rm tot}$=130, $N_R^{\rm int}$=48, $N_{r_2}^{\rm int}$=23, $N_{r_2}^{\rm asy}$=3, N_{r_3}=3
	$j_{1\rm max}$=20, $j_{23\rm max}$=36, $j_{3\rm max}$=26, $l_{2\rm max}$=32, $J_{\rm max}$=30
Initial wave packet	R_0=8.5, δ=0.12, E_i=0.4 eV
Damping term	R_a=9.0, α_R=0.05, n_R=2.5, r_{2a}= 3.4,α_{r_2}=0.035, n_{r_2}=2.0
Flux position	$r_2^{\rm F}$=3.0

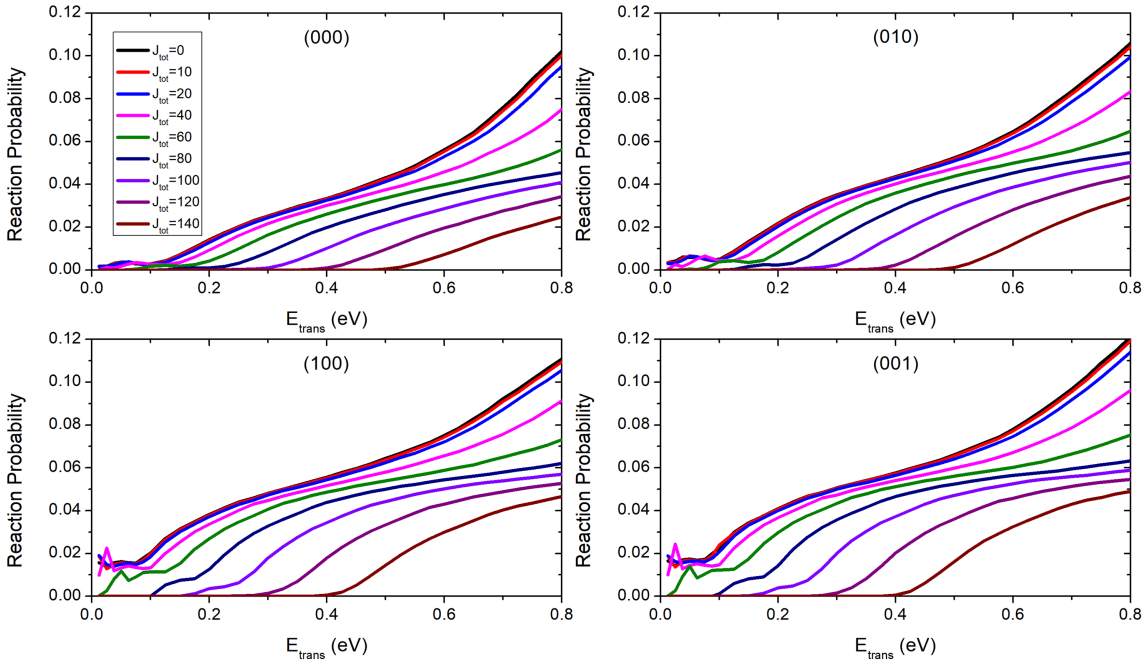

FIG. 3 Reaction probabilities of the reaction OH+$H_2S(n_1, n_2, n_3)$→H_2O+SH with $J_{\rm tot}$=0−140. Each vibrational state of H_2S is assigned by the three quantum numbers (n_1, n_2, n_3), representing excitations in the symmetric stretching, bending, and antisymmetric stretching modes, respectively.

each $J_{\rm tot}$ is similar to the corresponding curve from the reactant ground state except that the plateau appearing in the (010) state is slightly higher. The probability curve for exciting the symmetric stretching mode (100) resembles the antisymmetric (001) one. The plateau appearing in the lower panel, in which the reaction probability varies around 0.017, is visibly higher than the corresponding one from the (000) or (010) state. It is worth noting that there exists a peak at $E_{\rm trans}$=0.025 eV (0.05 eV) in the curve with $J_{\rm tot}$=40 (60), which possibly arises from resonance. The confirmation of the resonance in the reaction requires exact quantum scattering calculations in full-dimensional model, which, however, is beyond our computational capabilities.

The upper panel of FIG. 4 depicts the calculated ICSs from the first several vibrational states of H_2S as a function of collision energy. The calculated fundamentals of H_2S, (100), (010), and (001), are 2615, 1182, and 2624 cm^{-1}, which consist well with the experimental values of 2614, 1183, and 2628 cm^{-1} [51]. The ICS from the reactant ground state first oscillates at around 0.45 a_0^2, and then begins to rise up as the collision energy increases higher than 0.125 eV. The collision energy dependence of the ICS from either the fundamental or first overtone excitation of the bending mode is similar to that from the ground vibrational state. Impressively, when the stretching mode ((100) or (001)) is excited, the ICS first descends sharply with the increase of the collision energy, and then rises monotonically. Therefore, the reaction has a character of barrier-less reaction

DOI:10.1063/1674-0068/cjcp2112278

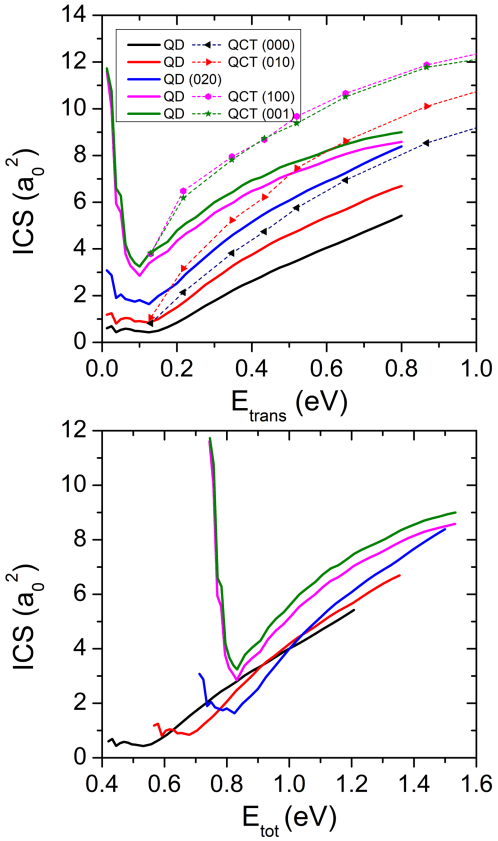

FIG. 4 Integral cross sections of the reaction OH+H_2S (n_1=0, 1, n_2=0, 1, 2, n_3=0, 1)→H_2O+SH, together with the earlier QCT results from Ref.[33].

in the energy range below around 0.1 eV, in which the ICS decreases as the collision energy increases. As the collision energy increases to above 0.1 eV, the reaction behaves like an activated reaction, in which the ICS increases with the collision energy. In addition, exciting each vibrational mode of H_2S enhances the reactivity over the energy range studied, with the stretching mode having higher efficacy. The previous QCT ICSs [33] are presented in the upper panel of FIG. 4 as well. Since the collision energy in the QCT calculations ranging from 0.13 eV to 1.0 eV is beyond the energy region where the pre-reaction wells dominate the reaction, the obtained ICS from each vibrational state rises up monotonically as the collision energy increases and exciting each stretching mode of H_2S enhances the reaction more efficiently than exciting the bending mode. These dynamical features are in accord with the QD findings.

In the lower panel of FIG. 4, the QD ICSs are plotted as functions of total energies. The efficacy for different kinds of energy on enhancing the reactivity depends subtly on the collision energy. Exciting the antisymmetric stretching mode has comparable efficacy with exciting the symmetric stretching mode with low and high collision energies, whose efficacies are higher than the bending mode, and the translational mode has the lowest efficacy. At middle energies, the efficacy of the translational energy becomes in between the stretching mode and the bending mode. The Sudden Vector Projection (SVP) model [52, 53] has been widely used to predict mode specificities in chemical reactions. The efficacy of a reactant mode in enhancing the reaction is estimated by the coupling strength between its normal mode and the reaction coordinate at the transition state (TS). The validity of the SVP model in predicting the mode specificity is in the condition that the intramolecular vibrational energy redistribution of reactants is much slower than the collision time and the TS plays a key role in the dynamics. As mentioned above, previous QCT calculations [33] have proved that there exist strong stereodynamics effects in the reaction. The initial orientation of reactants for most of reactive trajectories is toward the TS geometry. Therefore, the TS is thought to be a bottleneck of the reaction although the classical barrier is submerged. The calculated SVP value for each mode is given as follows: 0.00 (ν_{OH}), 0.31 (ν_{sym}), 0.09 (ν_{bend}), 0.28 (ν_{asym}), 0.39 (ν_{trans}). The OH vibrational mode has a projection of 0, indicating that it has a vanishing coupling with the reaction coordinate. The symmetric and antisymmetric stretching modes of H_2S have a projection of 0.31 and 0.28, respectively. Both of them are larger than the value of the bending mode (0.09), predicting that the stretching modes have higher efficacy than the bending mode on promoting the reaction. This is consistent with the QD results. The translational mode has the largest projection on the reaction coordinate with a value of 0.39. It implies that the translational energy enhances the reactivity more than the vibrational energy of H_2S, which is, however, not supported by the QD calculations.

FIG. 5 shows the initial state-specific rate constants of the OH+H_2S→H_2O+SH reaction in the temperature region from 200 K to 2000 K. The available experimental [17, 19−22, 54] and QCT [33] values are presented in the figure as well for comparison. Clearly, the rate constant from each state exhibits non-Arrhenius temperature dependence. The thermal averaged rate constant, which is obtained by Boltzmann averaging of the first five vibrational state-specific rate constants, is considerably smaller than the corresponding experimental

DOI:10.1063/1674-0068/cjcp2112278

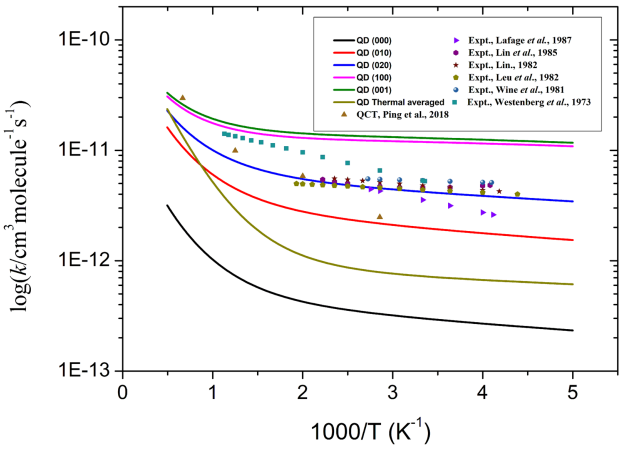

FIG. 5 Comparison of the theoretical and experimental thermal rate constants for the reaction OH+H_2S→H_2O+SH.

value. Considering that the QCT thermal rate constant on the same PES agrees reasonably well with the experimental value, the discrepancy is not thought to be caused by the inaccuracy of the PES. It is expected that the reactant rotational excitation has a significant contribution to the thermal rate constant, which, however, is not considered in this work.

IV. CONCLUSION

The ISSTDWP method is employed to study the dynamics and kinetic of the OH+H_2S→H_2O+SH reaction on an accurate PES. The bond distance of the reactant OH is fixed in the QD calculations, resulting in an eight-dimensional model. The reaction has a submerged classical barrier and a positive ZPE-corrected barrier. QD calculations show that the reaction behaves like a barrier-less reaction in the low energy range, where the integral cross section oscillates or decreases with the increase of the collision energy. However, the reaction manifests as an activated reaction with the collision energy higher than 0.1 eV, in which the ICS increases with the collision energy. The efficacy for the fundamental excitation of the symmetric stretching mode of H_2S is close to the antisymmetric stretching mode on promoting the reaction, which are higher than exciting the bending mode. The mode specificity is partially rationalized by the SVP model. Furthermore, the calculated state-specific rate constant presents a remarkable non-Arrhenius temperature dependence.

V. ACKNOWLEDGMENTS

This work was supported by the National Natural Science Foundation of China (No.21973109 to Hongwei Song, No.21773297, No.21973108, and No.21921004 to Minghui Yang) and the Ministry of Education, Singapore, under its Academic Research Fund Tier 1 (RG83/20) to Yunpeng Lu.

[1] G. Czakó and J. M. Bowman, J. Phys. Chem. A **118**, 2839 (2014).
[2] D. H. Zhang and H. Guo, Annu. Rev. Phys. Chem. **67**, 135 (2016).
[3] K. Liu, Annu. Rev. Phys. Chem. **67**, 91 (2016).
[4] H. Guo and K. Liu, Chem. Sci. **7**, 3992 (2016).
[5] B. Fu, X. Shan, D. H. Zhang, and D. C. Clary, Chem. Soc. Rev. **46**, 7625 (2017).
[6] H. Pan, K. Liu, A. Caracciolo, and P. Casavecchia, Chem. Soc. Rev. **46**, 7517 (2017).
[7] W. L. Hase, R. J. Duchovic, X. Hu, A. Komornicki, K. F. Lim, D. H. Lu, G. H. Peslherbe, K. N. Swamy, S. R. Vande Linde, A. Varandas, H. Wang and R. J. Wolf, Quantum Chem. Program Exch. Bull. **16**, 43 (1996).
[8] W. Stumm and J. J. Morgan, *Aquatic Chemistry*. New York: Wiley, (1996).
[9] C. F. Cullis and M. M. Hirschler, Atmosph. Environ. **14**, 1263 (1980).
[10] D. Möller, Atmosph. Environ. **18**, 19 (1984).
[11] D. R. Hitchcock, J. Air Pollu. Control Assoc. **26**, 210 (1976).
[12] T. E. Graedel, Rev. Geophys. **15**, 421 (1977).
[13] R. O. Beauchamp, J. S. Bus, J. A. Popp, C. J. Boreiko, D. A. Andjelkovich, and P. Leber, CRC Crit. Rev. Toxicol. **13**, 25 (1984).
[14] W. Jaeschke, H. Claude, and J. Herrmann, J. Geophys. Res.: Oceans **85**, 5639 (1980).
[15] M. Frenklach, J. H. Lee, J. N. White, and W. C. Gardiner, Combust. Flame **41**, 1 (1981).
[16] I. A. Gargurevich, Ind. Eng. Chem. Res. **44**, 7706 (2005).
[17] A. A. Westenberg and N. deHaas, J. Chem. Phys. **59**, 6685 (1973).
[18] R. A. Perry, R. Atkinson, and J. N. Pitts, J. Chem. Phys. **64**, 3237 (1976).
[19] P. H. Wine, N. M. Kreutter, C. A. Gump, and A. R. Ravishankara, J. Phys. Chem. **85**, 2660 (1981).
[20] C. L. Lin, Int. J. Chem. Kinet. **14**, 593 (1982).
[21] Y. L. Lin, N. S. Wang, and Y. P. Lee, Int. J. Chem. Kinet. **17**, 1201 (1985).
[22] C. Lafage, J. F. Pauwels, M. Carlier, and P. Devolder, J. Chem. Soc. Faraday Trans. **283**, 731 (1987).

DOI:10.1063/1674-0068/cjcp2112278

[23] H. Wang, D. Zhu, W. Wang, and Y. Mu, Chin. Sci. Bull. **55**, 2951 (2010).
[24] C. Wilson and D. M. Hirst, J. Chem. Soc. Faraday Trans. **90**, 3051 (1994).
[25] S. H. Mousavipour, M. A. Namdar-Ghanbari and L. Sadeghian, J. Phys. Chem. A **107**, 3752 (2003).
[26] B. A. Ellingson and D. G. Truhlar, J. Am. Chem. Soc. **129**, 12765 (2007).
[27] B. Du and W. Zhang, Comput. Theor. Chem. **1069**, 77 (2015).
[28] N. I. Butkovskaya and D. W. Setser, J. Phys. Chem. A **102**, 6395 (1998).
[29] N. I. Butkovskaya and D. W. Setser, Int. J. Chem. Kinet. **53**, 702 (2021).
[30] B. Wang, H. Hou, and Y. Gu, J. Mol. Struct.: THEOCHEM **505**, 241 (2000).
[31] B. Alday, R. Johnson, J. Li, and H. Guo, Theor. Chem. Acc. **133**, 1540 (2014).
[32] M. Tang, X. Chen, Z. Sun, Y. Xie, and H. F. Schaefer, J. Phys. Chem. A **121**, 9136 (2017).
[33] L. Ping, Y. Zhu, A. Li, H. Song, Y. Li, and M. Yang, Phys. Chem. Chem. Phys. **20**, 26315 (2018).
[34] K. Shao, J. Chen, Z. Zhao, and D. H. Zhang, J. Chem. Phys. **145**, 071101 (2016).
[35] L. Ping, L. Tian, H. Song, and M. Yang, J. Phys. Chem. A **122**, 6997 (2018).
[36] J. Z. H. Zhang, *Theory and Application of Quantum Molecular Dynamics*, Singapore: World Scientific, (1999).
[37] D. Wang, J. Chem. Phys. **124**, 201105 (2006).
[38] M. Yang, J. Chem. Phys. **129**, 064315 (2008).
[39] H. Song, J. Li, M. Yang, Y. Lu, and H. Guo, Phys. Chem. Chem. Phys. **16**, 17770 (2014).
[40] D. H. Zhang and J. Z. H. Zhang, J. Chem. Phys. **99**, 5615 (1993).
[41] R. T. Pack, J. Chem. Phys. **60**, 633 (1974).
[42] P. McGuire and D. J. Kouri, J. Chem. Phys. **60**, 2488 (1974).
[43] J. A. Fleck Jr., J. R. Morris, and M. D. Feit, Appl. Phys. **10**, 129 (1976).
[44] W. H. Miller, S. D. Schwartz, and J. W. Tromp, J. Chem. Phys. **79**, 4889 (1983).
[45] H. Song, A. Li, and H. Guo, J. Phys. Chem. A **120**, 4742 (2016).
[46] H. Song, A. Li, H. Guo, Y. Xu, B. Xiong, Y. C. Chang, and C. Y. Ng, Phys. Chem. Chem. Phys. **18**, 22509 (2016).
[47] L. Tian, Y. Zhu, H. Song, and M. Yang, Phys. Chem. Chem. Phys. **21**, 11385 (2019).
[48] D. Lu, J. Li, and H. Guo, Chem. Sci. **10**, 7994 (2019).
[49] Y. Liu, H. Song, D. Xie, J. Li, and H. Guo, J. Am. Chem. Soc. **142**, 3331 (2020).
[50] M. Pan, H. Xiang, Y. Li, and H. Song, Phys. Chem. Chem. Phys. **23**, 17848 (2021).
[51] A. D. Bykov, O. V. Naumenko, M. A. Smirnov, L. N. Sinitsa, L. R. Brown, J. Crisp, and D. Crisp, Can. J. Phys. **72**, 989 (1994).
[52] B. Jiang and H. Guo, J. Am. Chem. Soc. **135**, 15251 (2013).
[53] H. Guo and B. Jiang, Acc. Chem. Res. **47**, 3679 (2014).
[54] M. T. Leu and R. H. Smith, J. Phys. Chem. **86**, 73 (1982).

DOI:10.1063/1674-0068/cjcp2112278